

Tailored surface birefringence by femtosecond laser assisted wet etching

Rokas Drevinskas,^{1,*} Mindaugas Gecevičius,¹ Martynas Beresna,¹ Yves Bellouard² and Peter G. Kazansky¹

¹Optoelectronics Research Centre, University of Southampton, SO17 1BJ, United Kingdom

²Mechanical Engineering Department, Eindhoven University of Technology, P.O. Box 513, 5600 MB, Eindhoven, The Netherlands

*rd1c12@orc.soton.ac.uk

Abstract: Surface texturing is demonstrated by the combination of wet etching and ultrafast laser nanostructuring of silica glass. Using potassium hydroxide (KOH) at room temperature as an etchant of laser modified glass, we show the polarization dependent linear increase in retardance reaching a threefold value within 25 hours. The dispersion control of birefringence by the etching procedure led to achromatic behaviour over the entire visible spectral range. The mechanism of enhanced KOH etching selectivity after femtosecond laser exposure is discussed and correlated to the formation of various laser-induced defects, such as silicon-rich oxygen deficiency and color centers.

©2015 Optical Society of America

OCIS codes: (140.3390) Laser materials processing; (260.5430) Polarization; (260.1440) Birefringence.

References and links

1. R. R. Gattass and E. Mazur, "Femtosecond laser micromachining in transparent materials," *Nat. Photonics* **2**(4), 219–225 (2008).
2. Y. Shimotsuma, P. G. Kazansky, J. Qiu, and K. Hirao, "Self-organized nanogratings in glass irradiated by ultrashort light pulses," *Phys. Rev. Lett.* **91**(24), 247405 (2003).
3. R. Taylor, C. Hnatovsky, and E. Simova, "Applications of femtosecond laser induced self-organized planar nanocracks inside fused silica glass," *Laser Photon. Rev.* **2**(1-2), 26–46 (2008).
4. J. Canning, M. Lancry, K. Cook, A. Weickman, F. Brisset, and B. Poumellec, "Anatomy of a femtosecond laser processed silica waveguide [Invited]," *Opt. Mater. Express* **1**(5), 998 (2011).
5. V. Oliveira, S. P. Sharma, P. Herrero, and R. Vilar, "Transformations induced in bulk amorphous silica by ultrafast laser direct writing," *Opt. Lett.* **38**(23), 4950–4953 (2013).
6. M. Beresna, M. Gecevičius, and P. G. Kazansky, "Polarization sensitive elements fabricated by femtosecond laser nanostructuring of glass," *Opt. Mater. Express* **1**(4), 783–795 (2011).
7. J. Zhang, M. Gecevičius, M. Beresna, and P. G. Kazansky, "Seemingly unlimited lifetime data storage in nanostructured glass," *Phys. Rev. Lett.* **112**(3), 033901 (2014).
8. A. Marcinkevičius, S. Juodkazis, M. Watanabe, M. Miwa, S. Matsuo, H. Misawa, and J. Nishii, "Femtosecond laser-assisted three-dimensional microfabrication in silica," *Opt. Lett.* **26**(5), 277–279 (2001).
9. Y. Bellouard, A. Said, M. Dugan, and P. Bado, "Fabrication of high-aspect ratio, micro-fluidic channels and tunnels using femtosecond laser pulses and chemical etching," *Opt. Express* **12**(10), 2120–2129 (2004).
10. S. Juodkazis, K. Yamasaki, V. Mizeikis, S. Matsuo, and H. Misawa, "Formation of embedded patterns in glasses using femtosecond irradiation," *Appl. Phys., A Mater. Sci. Process.* **79**(4-6), 1549–1553 (2004).
11. C. Hnatovsky, R. S. Taylor, E. Simova, P. P. Rajeev, D. M. Rayner, V. R. Bhardwaj, and P. B. Corkum, "Fabrication of microchannels in glass using focused femtosecond laser radiation and selective chemical etching," *Appl. Phys., A Mater. Sci. Process.* **84**(1-2), 47–61 (2006).
12. M. Hörstmann-Jungemann, J. Gottmann, and D. Wortmann, "Nano- and microstructuring of SiO₂ and sapphire with fs-laser induced selective etching," *J. Laser Micro/Nanoeng.* **4**, 135–140 (2009).
13. F. Venturini, M. Sansotera, R. M. Vazquez, R. Osellame, G. Cerullo, and W. Navarrini, "Micromanufacturing in fused silica via femtosecond laser irradiation followed by gas-phase chemical etching," *Micromachines* **3**(4), 604–614 (2012).
14. C. Corbari, A. Champion, M. Gecevičius, M. Beresna, Y. Bellouard, and P. G. Kazansky, "Femtosecond versus picosecond laser machining of nano-gratings and micro-channels in silica glass," *Opt. Express* **21**(4), 3946–3958 (2013).

15. C. Hnatovsky, R. S. Taylor, E. Simova, V. R. Bhardwaj, D. M. Rayner, and P. B. Corkum, "Polarization-selective etching in femtosecond laser-assisted microfluidic channel fabrication in fused silica," *Opt. Lett.* **30**(14), 1867–1869 (2005).
16. Y. Bellouard, A. Said, and P. Bado, "Integrating optics and micro-mechanics in a single substrate: a step toward monolithic integration in fused silica," *Opt. Express* **13**(17), 6635–6644 (2005).
17. Y. Hanada, K. Sugioka, H. Kawano, I. S. Ishikawa, A. Miyawaki, and K. Midorikawa, "Nano-aquarium for dynamic observation of living cells fabricated by femtosecond laser direct writing of photostructurable glass," *Biomed. Microdevices* **10**(3), 403–410 (2008).
18. S. Juodkazis, V. Mizeikis, and H. Misawa, "Three-dimensional microfabrication of materials by femtosecond lasers for photonics applications," *J. Appl. Phys.* **106**(5), 051101 (2009).
19. S. Ho, M. Haque, P. R. Herman, and J. S. Aitchison, "Femtosecond laser-assisted etching of three-dimensional inverted-woodpile structures in fused silica," *Opt. Lett.* **37**(10), 1682–1684 (2012).
20. Y. Bellouard, E. Barthel, A. A. Said, M. Dugan, and P. Bado, "Scanning thermal microscopy and Raman analysis of bulk fused silica exposed to low-energy femtosecond laser pulses," *Opt. Express* **16**(24), 19520–19534 (2008).
21. S. Rajesh and Y. Bellouard, "Towards fast femtosecond laser micromachining of fused silica: The effect of deposited energy," *Opt. Express* **18**(20), 21490–21497 (2010).
22. S. Juodkazis, Y. Nishi, and H. Misawa, "Femtosecond laser-assisted formation of channels in sapphire using KOH solution," *Phys. Status Solidi-R* **2**(6), 275–277 (2008).
23. S. Kiyama, S. Matsuo, S. Hashimoto, and Y. Morihira, "Examination of etching agent and etching mechanism on femtosecond laser microfabrication of channels inside vitreous silica substrates," *J. Phys. Chem. C* **113**(27), 11560–11566 (2009).
24. S. LoTurco, R. Osellame, R. Ramponi, and K. C. Vishnubhatla, "Hybrid chemical etching of femtosecond laser irradiated structures for engineered microfluidic devices," *J. Micromech. Microeng.* **23**(8), 085002 (2013).
25. M. Hermans, J. Gottmann, and F. Riedel, "Selective, laser-induced etching of fused silica at high scan-speeds using KOH," *J. Laser Micro/Nanoeng.* **9**, 126–131 (2014).
26. M. Beresna, M. Gecevičius, M. Lancry, B. Poumellec, and P. G. Kazansky, "Broadband anisotropy of femtosecond laser induced nanogratings in fused silica," *Appl. Phys. Lett.* **103**(13), 131903 (2013).
27. D. J. Stokes, *Principles and practice of variable pressure/environmental scanning electron microscopy (VP-ESEM)* (John Wiley & Sons, Ltd, 2008).
28. A. Champion, M. Beresna, P. Kazansky, and Y. Bellouard, "Stress distribution around femtosecond laser affected zones: effect of nanogratings orientation," *Opt. Express* **21**(21), 24942–24951 (2013).
29. P. M. Dove, N. Han, A. F. Wallace, and J. J. De Yoreo, "Kinetics of amorphous silica dissolution and the paradox of the silica polymorphs," *Proc. Natl. Acad. Sci. U.S.A.* **105**(29), 9903–9908 (2008).
30. J. Gratz and P. Bird, "Quartz dissolution : theory of rough and smooth surfaces," *Geochim. Cosmochim. Acta* **57**(5), 977–989 (1993).
31. L. Skuja, "Optically active oxygen-deficiency-related centers in amorphous silicon dioxide," *J. Non-Cryst. Solids* **239**(1-3), 16–48 (1998).
32. H. Seidel, L. Csepregi, A. Heuberger, and H. Boumgortel, "Anisotropic etching of crystalline silicon in alkaline solutions," *J. Electrochem. Soc.* **137**(11), 3612–3626 (1990).
33. J. Kerr, *Handbook of chemistry and physics*, 81st ed. (CRC, 2000).
34. M. Gecevičius, M. Beresna, J. Zhang, W. Yang, H. Takebe, and P. G. Kazansky, "Extraordinary anisotropy of ultrafast laser writing in glass," *Opt. Express* **21**(4), 3959–3968 (2013).
35. H. Kikuta, Y. Ohira, and K. Iwata, "Achromatic quarter-wave plates using the dispersion of form birefringence," *Appl. Opt.* **36**(7), 1566–1572 (1997).
36. M. Gecevičius, M. Beresna, and P. G. Kazansky, "Polarization sensitive camera by femtosecond laser nanostructuring," *Opt. Lett.* **38**(20), 4096–4099 (2013).
37. N. Yu and F. Capasso, "Flat optics with designer metasurfaces," *Nat. Mater.* **13**(2), 139–150 (2014).

1. Introduction

Femtosecond laser assisted micro-machining through the nonlinear light-matter interaction attracts considerable interest due to its ability to produce three-dimensional devices in transparent media [1]. Under certain conditions, the interaction of femtosecond pulses with silica is known to induce self-assembled nanostructure with stripe-like oxygen deficient regions oriented perpendicular to the incident beam polarization [2]. The recent works suggested these regions being a composition of parallel planar nanocracks [3] or nanoporous planes filled with decomposed SiO₂ and oxygen [4] with silica nanocrystals of 4 nm size embedded in the defect-rich nanograting planes [5].

The sub-wavelength periodicity of ultrafast laser induced nanostructures behaves as a uniaxial birefringent material where the optical axis is parallel to the direction of laser polarization. The sign of birefringence is negative, according to planar form birefringence, with the typical value of -4×10^{-3} estimated in silica glass. For comparison, quartz is a

positive uniaxial crystal with the value of 9×10^{-3} . The birefringence resulting from self-assembled nanostructures in fused silica is exploited for the fabrication of numerous polarization sensitive optical elements ranging from diffraction gratings to polarization and optical vortex converters, and data storage [6,7].

More than a decade ago, it was demonstrated that the structure modification with ultrafast laser irradiation allows a highly selective wet etching process [8]. Generally, the etching is performed with diluted hydrofluoric acid (HF), which was successfully applied in fabrication of micro-channels, and tunnels [3,9–15] or more complex structures [8,16–19].

HF is a strong etchant even for pristine glass, therefore the etching rate and selectivity is mainly determined by the contrast in morphology of the laser modified, i.e. locally induced stress or nanocracks, and unmodified zones [3,20]. The typical HF based micro-fabrication gives the etching ratio up to 50 [21]. To enhance the selectivity, a promising alternative for HF is potassium hydroxide (KOH) [21–25]. The mechanism for femtosecond laser assisted KOH etching of fused silica is still under debate and a few studies can be found on the matter. It is suggested that KOH efficiently tackles laser induced Si-rich structures while the SiO₂ matrix remains almost unetched, giving the ratio up to 200 for micro-channel fabrication at high etchant temperatures (80°C) [23].

In this paper, we demonstrate that selective KOH etching reveals high contrast nanogratings without affecting the unmodified silica lattice and leads to the control of optical dispersion and enhancement of the retardance exhibited by the nanostructures.

2. Laser assisted KOH etching of fused silica

In order to investigate the laser assisted etching process, several millimetre long lines were written with a regeneratively amplified, mode-locked Yb:KGW based ultrafast laser system (Pharos, Light Conversion Ltd.) operating at 1030 nm at a 200 kHz-repetition rate. Two identical samples were prepared using pulse duration of 700 fs, a linear polarization oriented perpendicular to the writing direction, a writing speed of 0.2 mm/s and a pulse energy of 2.5 μJ. The laser beam was focused in the bulk of the silica substrate using a 0.16 NA-objective lens yielding a fluence of roughly 19 J/cm². After the laser irradiation, nanoplanes parallel to the laser beam propagation and perpendicular to the polarization plane were formed. To reveal the nanograting cross-section, the sample was lapped and polished.

Taking into account that laser-induced defects [oxygen deficiency centers (ODC II, = Si⁰) and color centers (E', ≡Si[•])] tend to annihilate at high temperatures [26], one sample was annealed at 900°C for one hour while the other was kept at room temperature. Both the annealed and non-annealed substrates were then immersed into a KOH (1 mol/L) solution at room temperature (RT, 20° C) for 24 hours.

Surface imaging during all fabrication steps was performed with a scanning electron microscope (SEM) (Zeiss Evo50 and Zeiss Evo ME15) operating in two modes: (1) high-vacuum secondary electron mode (SE) and (2) variable pressure environmental scanning electron mode (VP-ESEM or VPSE), collecting the luminescence signal by excitation-relaxation and electron-ion recombination of molecules in gaseous chamber [27].

VPSE mode enables high-resolution scanning without conductive coating and additional surface etching. In the microscope chamber, gas molecules are ionized via the interaction with primary, backscattered and secondary electrons. After a short time, on the nanosecond scale, the excited molecules relax to the neutral ground state, emitting photons. This transition is caused due to a short lifetime of the excited state and electron-ion recombination, when the electrons emitted from the specimen or generated in the gas cascade are captured by the ions. Due to a strong electric field in the chamber, ionized gas molecules are attracted to the sample and recombined with the surface electrons, mapping its insulator/conductor properties via a luminescence signal. The better insulator the sample is, the more electrons are built-up and are emitted [27]. As a result, the regions with more constrained electrons in the VPSE image appear brighter and vice versa.

As can be seen in Fig. 1 (a) and (c), after the twenty four hours annealing procedure, some part of the nano-structures visible in the VPSE image of non-annealed specimens disappeared. Indeed, images of non-annealed nanograting show the nanoplanes as dark regions surrounded by a white shell while their annealed counter-parts show only a white pattern. Considering the physical principle of the VPSE imaging mode, the observation points toward a localized increase of surface conductivity that disappear during the annealing process. Knowing that ODC (II) and E' defects annihilate, we conclude that these oxygen deficient-regions are the main reason for the locally increased surface conductivity. It should be noted that bright shells surrounding etched-grooves are caused by the built-up of electrons showing its tendency to localize in the higher density at the surface edges which further supports a model of localized volume expansion in the nanogratings regions [28]. The same specimens were then coated with a 10 nm gold layers and imaged using the topography based SE mode (Figs. 1(b) and 1(d)). It shows that the width of the etched planes shrinks by a factor of 2 from ~30 nm to ~15 nm. In the case of the annealed specimen, we attribute the ongoing KOH etching to the dissolution of $\equiv\text{Si}-\text{Si}\equiv$ bonds generated during laser exposure.

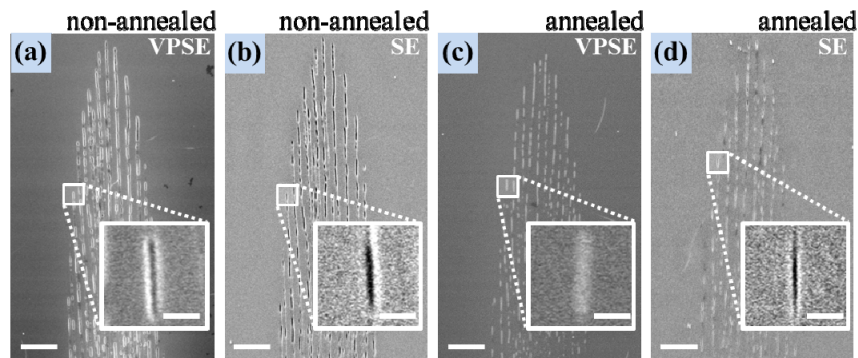
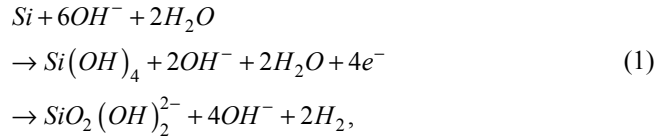


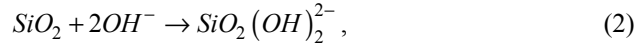
Fig. 1. SEM images of the cross sectioned single line nanograting, etched for 24 h: (a) non-annealed, imaged with VPSE mode; (b) non-annealed, imaged with SE mode; (c) annealed at 900°C for 1h, imaged with VPSE mode; (d) annealed at 900°C for 1h, imaged with SE mode. For SE mode samples were coated with a 10 nm-gold film. The insets show magnified defect-rich nanoplanes in laser modified silica. Scale bars are 2 μm for full images and 125 nm for insets.

Structurally, amorphous silica tetrahedra in the bulk consists of silica coordinated tetrahedras ($\equiv\text{Si}-\text{O}-\text{Si}\equiv$) with two- and three-fold coordinations with the surface [29,30]. In order to get a soluble complex, the dissolution of unmodified glass must be based on the termination of connection through the two or three Si-O backbond sites of the $\equiv\text{Si}-\text{O}-\text{Si}\equiv$ groups to the neighbouring atoms. After the femtosecond laser irradiation the various types of defects are induced: Si-rich oxygen deficiency centers ($\equiv\text{Si}-\text{Si}\equiv$ or ODC I); oxygen deficiency centers ($=\text{Si}^0$ or ODC II); color centers ($\equiv\text{Si}^{\cdot}$ or E') and non-bridging oxygen-hole centers ($\equiv\text{Si}-\text{O}^{\cdot}$ or NBOHC) [26,31]. In that case, the dissolution of laser modified glass is based on the termination of connection through the combination of zero to three Si-O and Si-Si backbond sites to the neighbouring atoms.

Considering pure crystalline silicon and silica glass composites, the etching selectivity at high temperatures ($\sim 100^\circ\text{C}$) gives values of about 100-300, while at RT the ratio increases by an order of magnitude giving the etching rate of 2-3 $\mu\text{m}/\text{h}$ for silicon and ~ 0.8 nm/h for silica [32]. The dissolution reaction mechanism [32] for pure Si is:



and for SiO₂ substrate, it is written:



These equations describe the processes under high pH of silicate (SiO₂(OH)₂²⁻) solutions (as well as orthosilicic acid (Si(OH)₄) for pure Si) in which potassium ions (K⁺) take part only by affecting the potential distribution in the electrolyte [32]. Both chemical reactions, described in Eqs. (1) and (2), yield the same final products through different paths (breaking of two and three Si–O (799 kJ mol⁻¹) backbond sites for SiO₂ substrates and Si–Si (326 kJ mol⁻¹ for native silicon and weaker for ≡Si–Si≡ defects) sites for Si substrates [33]).

For femtosecond laser-modified zones, we consider that the higher etching selectivity results from a combination of two effects, structural and morphological. On one hand, the femtosecond laser locally modifies the SiO₂ matrix introducing both backbond and dangling bond sites. On the other hand, the change in morphology directly affects the etching rate by increasing the surface area exposed to the etchant and therefore, available for chemical reaction. In the sequel, we use the high-selectivity of KOH etching to investigate birefringent surfaces.

3. Laser-induced surface birefringence

In these experiments, the silica glass was irradiated using the laser setup described before. The sample was modified with 300 fs and 700 fs pulses, polarized parallel (0°) and perpendicular (90°) to the writing direction. The writing speed was 1 mm/s with 0.5 μm interline distance and the laser pulse energy was in the range of 0.25–0.55 μJ. The laser beam was focused in the bulk of the substrate via a 0.35 NA objective lens providing a net fluence of 9–20 J/cm². For each set of parameters (polarization, pulse duration, and laser energy), 32 squares (of 100 μm-side dimension) were written at different depths (z-axis) starting from 75 μm and moving deeper by 1.5 μm steps (Fig. 2). A total of 512 squares were written.

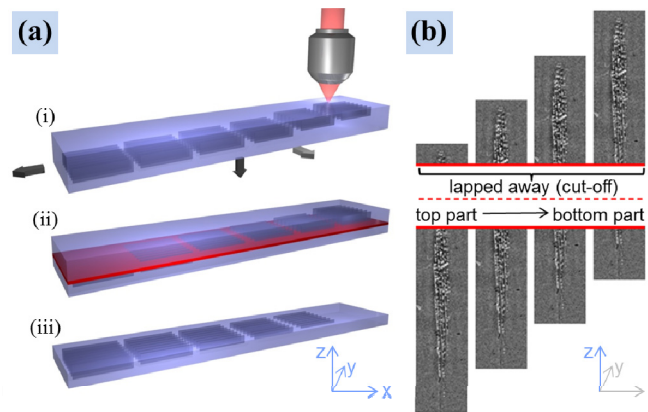


Fig. 2. (a) The sketch of laser-assisted fabrication of surface nanograting: (i) femtosecond laser writing inside a bulk glass, (ii) lapping and (iii) polishing. (b) Schematic diagram of the lapping, from the cross-sectioned single line nanograting point of view, showing the structure sectioning in z-axis direction.

For the laser processing conditions specified before, the 12 to 16 μm -long nanogratings were fabricated (z -axis direction). The top surface of the sample was lapped/polished (Logitech LP50) removing $80 \pm 5 \mu\text{m}$ of the material. As a result, the uppermost squares were completely cut-off and the lower structures were sectioned at different depths revealing different cross-sections of the nanograting (Fig. 2 and Fig. 3). The lowest squares remained unaffected inside the bulk of the substrate. The etching of the nanograting exposed on the surface was carried out at room temperature (RT, 20°C) by immersing the sample into a KOH solution (1 mol/L), for a specific period of time, varying from 5 minutes to 1 hour. After each time period, the sample was dried for subsequent characterizations.

The modified areas were characterized with a quantitative birefringence measurement system (CRi Abrio mounted on an Olympus microscope BX51) operating at 546 nm wavelength. The dispersion of retardance was measured using a VIS-NIR birefringence measurement system (CRAIC also mounted on an Olympus microscope BX51). The polarizer before the sample was fixed at a 45° angle with respect to the nanograting orientation, while the polarizer after the sample was rotated either to 45° or to -45° . The spectral measurements of transmitted light intensity were taken for two configurations of the setup, the first one being when both polarizers are parallel, (I_{parallel}) and the second one when polarizers are perpendicular one to another ('cross polarized', I_{crossed}). The retardance dispersion $R(\lambda)$ was then calculated as follows [26]:

$$R(\lambda) = a \cos\left(\frac{I_{\text{parallel}} - I_{\text{crossed}}}{I_{\text{parallel}} + I_{\text{crossed}}}\right) \cdot \frac{\lambda}{2\pi} = \Delta(\lambda) \cdot \frac{\lambda}{2\pi}. \quad (3)$$

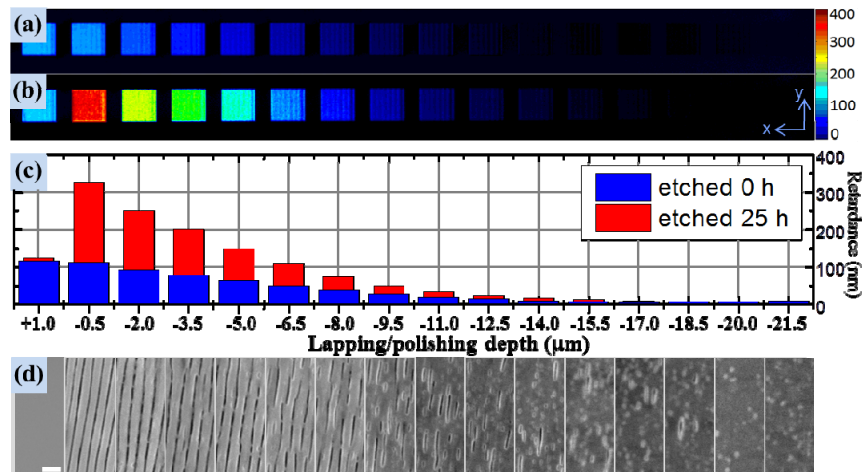


Fig. 3. The nanograting lapped/polished at different depths from $Z = +1.0 \mu\text{m}$ to $Z = -21.5 \mu\text{m}$, written with 300 fs, 0° polarization and $0.45 \mu\text{J}$ pulse energy (see Fig. 2). The peak part of the nanograting is at the depth of $Z = 0 \mu\text{m}$. (a), (b) Retardance (in air, for $\lambda = 546 \text{ nm}$) images before and after total 25 h etching, respectively, with the columns (c) indicating its values at different cut-off. Color scale: 0–400 nm. (d) VPSE SEM images of the sectioned and etched nanograting, where the cut-off values correspond to (a)–(c). Scale bar: 500 nm.

Within the first 60 min of the etching procedure, the retardance increase rate dropped almost by one order until it saturated and became constant over the rest time of the experiment (Figs. 4(a)–4(d)). The change of slope in the retardance growth after one hour is attributed to the initially high etching rate observed during the first hour. This increased etching rate can be explained by two factors: an easier access of the etchant to the modified, defects-rich, regions and the OH⁻ concentration decreasing in time. The second factor seems to be less dominant because continuous experiments without refreshing the etchant yield the same results as experiments performed with a continuous refreshing of the etchant. After total 25 hours of

etching, a three-fold retardance increase was observed for all experimental conditions with 0° incident beam polarization while a two-fold retardance increase was found for 90° polarization. In both cases, there is no indication of saturation, what suggests that further etching would lead to higher retardance level (Fig. 4). From the SEM-based analysis, we can see that the top 3 to 6 μm of the laser-induced structure contains highly-ordered nanopatterns (Fig. 3(d)) that provides a major contribution to the measured retardance value after the etching process (Figs. 3(a)–3(c)). Going down from the top to the bottom of the laser affected structures, the order and the continuity of nanoplanes are lost presumably due to an increase of the scattering. The uniform planes are fully replaced by randomly distributed porous structure at depth of 10 to 12 μm (Fig. 3(d)). For this reason, all the following results presented in this paper are related to the squares with the cut-off position – measured from the top of the laser induced zone - smaller than 1.5 μm .

Before the etching process, the retardance of laser induced nanogratings depends both on polarization and pulse duration. Pulses with 0.25 μJ -energy and 90° -polarization produce about 70% higher retardance values than with 0° -polarization without exhibiting a dependence on the pulse duration. Such a high difference in retardance is caused by the laser processing conditions close to the threshold for nanogratings formation ($\sim 0.2 \mu\text{J}$ [6]). For the higher pulse energy, the retardance difference decreases with the appearance of a dependence on pulse duration. In the case of 0.45 μJ and 0.55 μJ pulse energies with 700 fs-pulse duration, the induced nanograting possesses up to $\sim 40\%$ higher retardance values than with 300 fs showing only a weak dependence on polarization state [34]. However, during the etching experiment the birefringence exhibits strong dependence on polarization giving $\sim 50\%$ higher retardance increase for 0° polarization (Figs. 4(a)–4(d)) and show only a weak dependence on pulse duration (Fig. 5(a)).

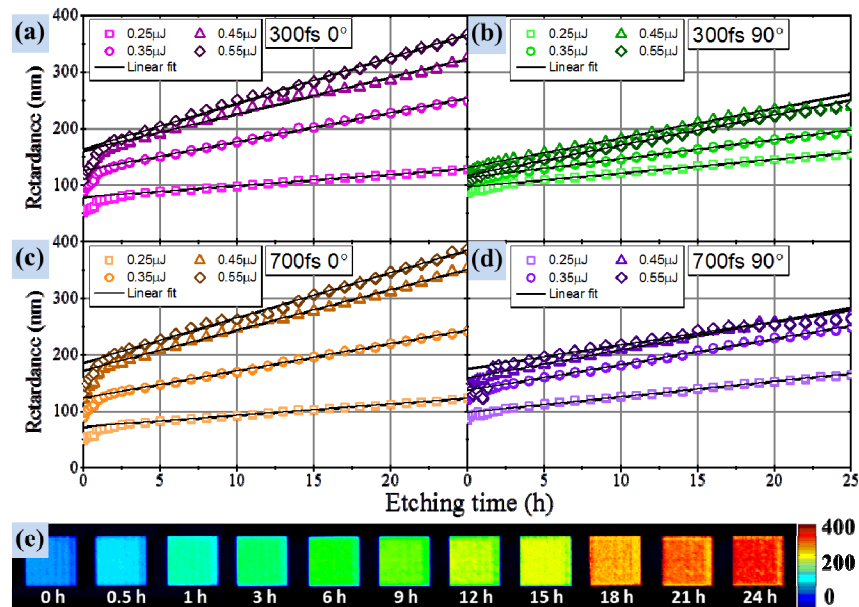


Fig. 4. (a)–(d) Retardance (in air, for $\lambda = 546 \text{ nm}$) dependence on the etching time. Nanograting was written with 700 fs and 300 fs pulse duration, 0° and 90° polarization, energies ranging from 0.25 μJ to 0.55 μJ ; lapped and polished at the top part of the structure. The linear fitting was performed. (e) Imaged retardance (in air, for $\lambda = 546 \text{ nm}$) dependence on the etching time. Structure was written with 300 fs, 0° polarization and 0.45 μJ pulse energy. Color scale: 0–400 nm.

The retardance exhibited by the exposed nanograting was linearly increasing with the etching time. The growth rates extracted from the linear fits of the etching kinetics (Fig. 4) group into two polarization branches (Fig. 5(a)). At 0.25 μJ the rates are higher for 90° polarization while at 0.35–0.55 μJ the 0° polarization bypasses it.

The formation of irregularities and periodic ruptures observed for 0.45–0.55 μJ and 90° polarization is believed to be the key factor for the roughly two times lower retardance growth rates observed after the etching process (Fig. 5(b)). It is more efficient to maintain the grating homogeneity assembling it into the orientation perpendicular to the writing direction (0° polarization) where each new written line extends the nanoplanes.

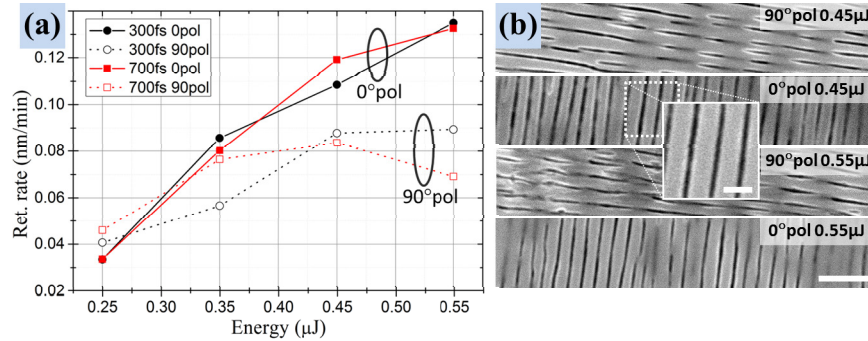


Fig. 5. (a) The etching induced retardance growth rate dependence on the laser modification conditions. The steady-state growth rates were extracted from the fitting curves, see Fig. 4. (b) VPSE SEM images of the surface nanograting written with 300 fs at various conditions and etched for 25 h. Inset shows the higher resolution zoomed in etched silica regions/nanoplanes. Scale bars: 1 μm and 300 nm (for inset).

The dispersion analysis revealed achromatic behaviour in the spectral range from 400 nm to 870 nm for the etched nanostructures induced with 0.45 μJ and 0.55 μJ pulse energies (Fig. 6(a)). In order to create achromatic birefringent device, the constant phase shift for all wavelengths must be ensured. Knowing that the element before the etching procedure was chromatic, we estimate that the retardance growth rate at 850 nm was almost two times larger than at 515 nm. After 25 h of etching, we get 1.2π – 1.4π phase shift in the spectral range from 400 to 870 nm.

In general, the etching process offers a method to control the retardance of the surface elements by removing laser modified silica regions, i.e. when defect-rich nanoplanes are dissolved. Subsequent control of the retardance is achieved by filling the surface nanostructure with water. The dispersion variation from air to water medium indicates a -3.22π – 3.30π phase shift per refractive index (RIU) with a refractive index resolution of $6 \cdot 10^{-3}$ (Fig. 6(b)). For a lower refractive index of the surrounding medium, a higher retardance is observed. In consequence, modified silica (defect-rich) regions before etching (“Bulk” line in Fig. 6(b)) have a lower refractive index than the water.

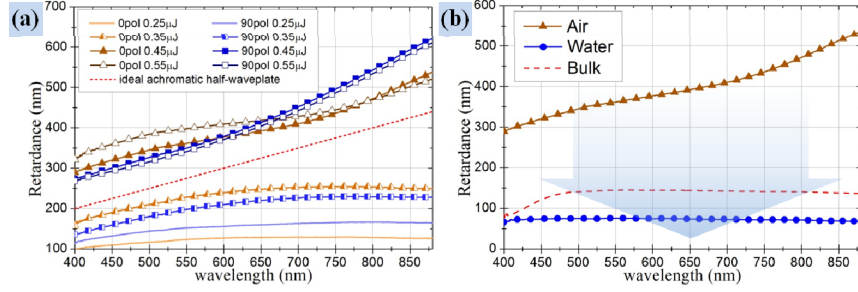


Fig. 6. Retardance (in air) dispersion of 25 h etched nanograting (a) written with 700 fs, energies from 0.25 μJ to 0.55 μJ and two polarizations states. (b) Retardance dispersion of nanograting filled with different refractive index medium: bulk – before etching (defect-rich silica); air – etched for 25 h and dried; water – etched for 25 h and immersed in water. The nanograting was written with 700 fs, 45 μJ pulse energy and 0° polarization. Blue arrow indicates the increase of medium's refractive index.

The qualitative analysis of the effective refractive indices change for TE and TM waves (n_{TE} and n_{TM}) was performed based on the so-called effective medium theory [35]

$$k_{1TE,1TM} = \sqrt{\left(\frac{2\pi n_1}{\lambda}\right)^2 - \beta_{TE, TM}^2}, \quad (4)$$

$$k_{2TE,2TM} = \sqrt{\left(\frac{2\pi n_2}{\lambda}\right)^2 - \beta_{TE, TM}^2}, \quad (5)$$

$$1 = \cos(a \cdot k_{1TE}) \cos(b \cdot k_{2TE}) - 0.5 \cdot \left(\frac{k_{2TE}}{k_{1TE}} + \frac{k_{1TE}}{k_{2TE}}\right) \sin(a \cdot k_{1TE}) \sin(b \cdot k_{2TE}), \quad (6)$$

$$1 = \cos(a \cdot k_{1TM}) \cos(b \cdot k_{2TM}) - 0.5 \cdot \left(\frac{n_1^2 k_{2TM}}{n_2^2 k_{1TM}} + \frac{n_2^2 k_{1TM}}{n_1^2 k_{2TM}}\right) \sin(a \cdot k_{1TM}) \sin(b \cdot k_{2TM}), \quad (7)$$

$$n_{TE, TM} = \frac{\lambda}{2\pi} \beta_{TE, TM}, \quad (8)$$

where n_1 and n_2 are the refractive indices of silica and variable medium (modified-silica, water or air), respectively defined with the duty cycle of $a/(a + b)$ (Fig. 7). The retardance can be determined by the structure depth (d) and the difference in the effective refractive indices:

$$R = d \cdot (n_{TE} - n_{TM}). \quad (9)$$

To simplify the calculations, we approximate laser induced nanogratings by an ideal cube shape with a constant order assembly along the entire depth of the structure (Fig. 7). Then, knowing the retardance value of the unetched nanograting, the total cube's depth (d) of 8 μm was estimated. The nanograting period (275 nm) and duty cycle (0.89) used in calculations were determined from the SEM analysis. Having all these parameters we could calculate retardance and refractive indices for layered medium by using Eqs. (4)–(9). The retardance values that are close to the experimentally measured ones, were obtained by reducing the refractive index of modified nanoplanes to $0.767 \cdot n_{\text{silica}}$. This correction factor takes into account the porous and defect-rich nature of the material forming the grooves.

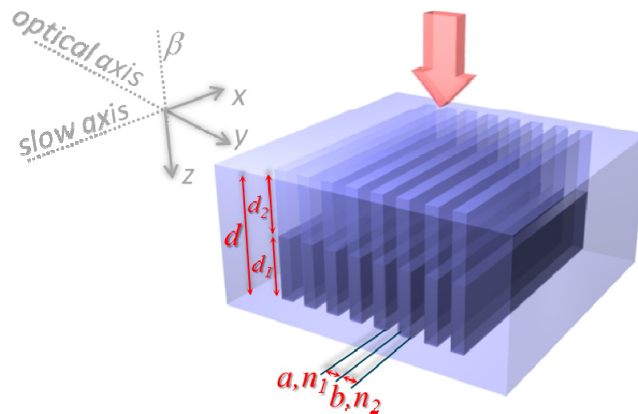


Fig. 7. The sketch of the light wave β (red arrow) propagating along the femtosecond laser induced nanograting in the silica glass. The optical axis of the fabricated birefringent element is perpendicular and the slow axis is parallel to the grating nanoplanes with thickness b and refractive index n_2 ; a and n_1 corresponds to the unmodified silica glass. The depth (d) of the nanograting is divided into unetched (d_1) and etched (d_2) parts.

Using the same modeling parameters, we analyzed the behavior of the etched nanograting filled with water. From the experimental results (Fig. 6(b)) we clearly see the chromatic retardance of ~ 75 nm. The corresponding calculations of modified-silica/silica (d_1 , bn_2/an_1) and water/silica (d_2 , bn_2/an_1) sandwiches indicate that water penetrates about $4.1 \mu\text{m}$ into the nanostructure and the water/silica part contributes only for ~ 9 nm of the total, 75 nm retardance.

Curiously, the calculations for air/silica produced a weak achromatic behavior and resulted in retardance much lower than observed in the experiments. We speculate that the achromatic properties of the structure are caused by the changing duty cycle and non-uniform/dispersive values of the effective refractive indices along the depth of the grating. The inconsistency between experiments and modeling in this particular case is attributed to these parameters that were not taken into account in the calculations.

4. Conclusions

We have demonstrated a fabrication method of birefringent surface elements in fused silica. Femtosecond laser-induced nanogratings written in the bulk of silica with 0° incident beam polarization exhibit up to a three-fold retardance increase after lapping/polishing and 25 h of KOH etching at room temperature. Scanning electron microscopy analysis before and after the annealing procedure indicates a strong relationship between a locally increased surface conductivity and laser-induced ODC (II) and E' defects that accounts for the high etching selectivity between modified and unmodified silica zones. The removal of sub-wavelength periodicity stripe-like oxygen deficient regions by etching and replacement with the different medium gives a way to effectively control the refractive indices of TM and TE waves. This observation opens new opportunities for designing both, chromatic and achromatic wave plates that can be used for micro-optics applications such as polarization sensitive cameras [36], and flat optics [37].

Acknowledgments

We are grateful to Dr. Stuart Boden for useful discussions in the field of scanning electron microscopy.